Quantifying garnet-melt trace element partitioning using lattice-strain theory: Assessment of statistically significant controls and a new predictive model

Draper, D.S.; van Westrenen, W.

published in
Contributions to Mineralogy and Petrology
2007

DOI (link to publisher)
10.1007/s00410-007-0235-3

document version
Publisher's PDF, also known as Version of record

Contrib Mineral Petrol (2007) 154:731–746
DOI 10.1007/s00410-007-0235-3

ORIGINAL PAPER

Quantifying garnet-melt trace element partitioning using lattice-strain theory: assessment of statistically significant controls and a new predictive model

David S. Draper · Wim van Westrenen

Received: 16 August 2006 / Accepted: 19 June 2007 / Published online: 19 July 2007

Abstract As a complement to our efforts to update and revise the thermodynamic basis for predicting garnet-melt trace element partitioning using lattice-strain theory (van Westrenen and Draper in Contrib Mineral Petrol, this issue), we have performed detailed statistical evaluations of possible correlations between intensive and extensive variables and experimentally determined garnet-melt partitioning values for trivalent cations (rare earth elements, Y, and Sc) entering the dodecahedral garnet X-site. We applied these evaluations to a database containing over 300 partition coefficient determinations, compiled both from literature values and from our own work designed in part to expand that database. Available data include partitioning measurements in ultramafic to basaltic to intermediate bulk compositions, and recent studies in Fe-rich systems relevant to extraterrestrial petrogenesis, at pressures sufficiently high such that a significant component of majorite, the high-pressure form of garnet, is present. Through the application of lattice-strain theory, we obtained best-fit values for the ideal ionic radius of the dodecahedral garnet X-site, $r_0(3+)$, its apparent Young's modulus $E(3+)$, and the strain-free partition coefficient $D_0(3+)$ for a fictive REE element J of ionic radius $r_0(3+)$. Resulting values of E, D_0, and r_0 were used in multiple linear regressions involving sixteen variables that reflect the possible influence of garnet composition and stoichiometry, melt composition and structure, major-element partitioning, pressure, and temperature. We find no statistically significant correlations between fitted r_0 and E values and any combination of variables. However, a highly robust correlation between fitted D_0 and garnet-melt Fe–Mg exchange and D_{Mg} is identified. The identification of more explicit melt-compositional influence is a first for this type of predictive modeling. We combine this statistically-derived expression for predicting D_0 with the new expressions for predicting E and r_0 outlined in the first of our pair of companion papers into an updated set of formulae that use easy-to-measure quantities (e.g. garnet composition, pressure, temperature) to predict variations in E, r_0, and D_0. These values are used in turn to calculate D values for those garnets. The updated model substantially improves upon a previous model (van Westrenen et al. in Contrib Mineral Petrol 142:219–234, 2001), and accounts well for trivalent cation partitioning in nominally anhydrous systems up to at least 15 GPa, including for eclogitic bulk compositions and for Fe-rich systems appropriate to magmagenesis on the Moon and Mars. The new model is slightly less successful in predicting partitioning with strongly majoritic garnets, although the mismatch is much less than with the original 2001 model. Although it also improves upon the 2001 model in predicting partitioning in hydrous systems, the mismatch between model and observation is still unacceptably large. The same statistical tools were applied in an attempt to predict tetravalent partitioning as well, because lattice-strain based techniques are not applicable to such partitioning. However, no statistically significant predictive relationships emerged from that effort. Our analyses show that future efforts should focus on filling the gap in partitioning data between ~10 and 25 GPa to evaluate more closely the gradual transition of garnet to majorite, and on

Communicated by T.L. Grove.

D. S. Draper (✉)
Institute of Meteoritics, 1 University of New Mexico,
MSC03-2050, Albuquerque, NM 87131, USA
e-mail: david@draper.name

W. van Westrenen
Faculty of Earth and Life Sciences, Vrije Universiteit,
De Boelelaan 1085, 1081 HV Amsterdam, The Netherlands

systematically expanding the hydrous partitioning database to allow extension of our model to water-bearing systems.

Introduction

In the first paper in this companion pair (van Westrenen and Draper, this issue), we reviewed progress made in updating the predictive model of van Westrenen et al. (2001b) for garnet-liquid trivalent trace element partitioning, referred to as *WvW01* hereafter, in terms of improved crystal-chemical and thermodynamic formulations made possible by the inclusion of new partitioning data produced since the initial publication of WvW01. The original model did not account for the presence of a majorite component in garnet, particularly in Fe-rich compositions typical of lunar and martian magmas (Draper et al. 2003, 2006; Dwarzski et al. 2006), leading to unacceptably large mismatches between model and observation. Figure 1 shows examples of these mismatches. This shortcoming has prompted our efforts to expand the database for garnet-melt partitioning, combining data we have produced for that purpose with those generated by other groups since WvW01. Success in this effort would allow the predictive model to be used to constrain the geochemical role of garnet in the generation of lunar and martian magmas, as well as those on Earth.

In this contribution, we augment the theoretical formulations presented by WvW01 and in van Westrenen and Draper (this issue) to include statistical evaluations of empirical relationships between garnet-melt partitioning

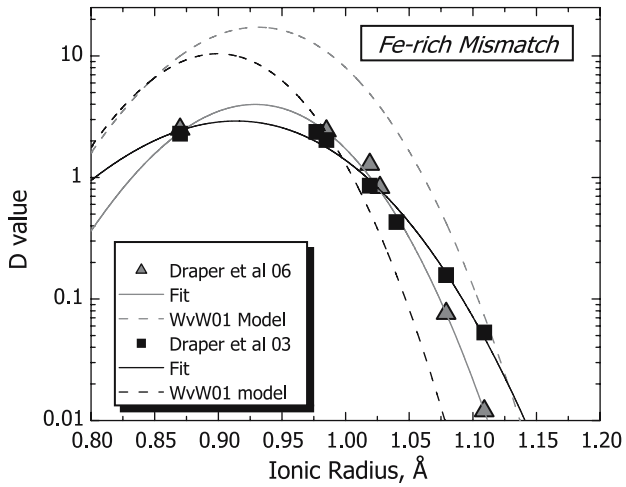

Fig. 1 Illustration of mismatch in Fe-rich systems between measured garnet-melt partitioning and that predicted by WvW01 model. Data are from experiments on Apollo 15 green C, a low-Ti lunar picrite glass composition (Draper et al. 2006) and on Homestead L5 ordinary chondrite (Draper et al. 2003). Solid curves are fits of data to Eq. 1, dashed curves are predictions given by WvW01 model

values for trivalent cations, as expressed by fits of experimental data to the lattice-strain equation, and parameters that are relatively easy to measure or estimate, such as garnet and melt major element compositions, pressure, and temperature. We define D values as the weight ratio of an element of interest between coexisting garnet and melt, i.e. $D = \text{concentration}^{\text{garnet}}/\text{concentration}^{\text{melt}}$, following the terminology of Beattie et al. (1993). We use D values to obtain values for E, the apparent Young's modulus of the garnet X-site, where trivalent trace elements such as the rare earth elements typically reside (Quartieri et al. 1999a, b; 2002), r_0, the ionic radius of the "ideal" trace element cation that dissolves into that site without straining the crystal lattice, and D_0, the maximum D value possible for a cation of a given charge (in this case, 3+) occupying that site. D values are related to these three parameters by the lattice-strain equation, first promulgated by Blundy and Wood (1994) and Wood and Blundy (1997) to rationalize plagioclase-melt and clinopyroxene-melt D values, and later applied to garnet in the WvW01 model:

$$D_i = D_0 \times \exp\left[\frac{-4\pi EN\left[\frac{r_0}{2}(r_i - r_0)^2 + \frac{1}{3}(r_i - r_0)^3\right]}{RT}\right], \quad (1)$$

where D_i is the measured partition coefficient for element i, r_i is the ionic radius of that element, R is the gas constant, N is Avogadro's number, and T is in Kelvin. This expression helps attach physical meaning to the long-known near-parabolic trends formed when D values for elements having the same charge, partitioning into the same crystallographic site, are plotted against ionic radius, as was first detailed by Onuma et al. (1968).

As was the case for the original WvW01 model, the goal of this work is to provide a means by which trivalent element partitioning between coexisting garnet and melt can be predicted from easy-to-evaluate parameters. In addition, we hope to elucidate constraints on the fundamental control(s) on D values: is it melt composition and structure, crystal composition, or both, and which has the largest effect? Some recent studies, e.g. Mysen and Dubinsky (2004) and Gaetani (2004), have raised questions about the lack of incorporation of an *explicit* term reflecting melt composition (and hence melt structure) in predictive models that use the lattice-strain approach. However, melt composition does play an *implicit* role in those models via the incorporation of terms such as D_{Mg} in WvW01, and D_{Fe} in the van Westrenen and Draper (this issue) formulation for predicting D_0 for trivalent cation partitioning between garnet and melt; similar but more complicated involvement appears in the predictive expressions for clinopyroxene presented by Wood and Blundy (1997). The success of

these models shows that incorporating such an explicit account does not appear to be *required* in lattice-strain expressions to obtain predictions of D values that are accurate enough to be used in geochemical modeling. One purpose of the addition of statistical assessments as presented here is to provide an opportunity for the explicit evaluation of the effect of melt composition and/or melt structure on partitioning, and then compare the accuracy of predictions resulting from both approaches.

We investigated a wide range of combinations of parameters to seek statistically significant correlations, and combined those results with the revised theoretical formulations presented in the first of this pair of companion papers to yield an updated model that successfully predicts anhydrous partitioning of trivalent cations to within a few tens of percent relative. As we show below, this approach provides a statistical expression for D_0 that performs as well as the D_0 expression formulated from thermodynamic considerations in van Westrenen and Draper (this issue), while requiring only two controlling parameters, D_{Mg} and garnet-melt Fe–Mg exchange. Both terms involve melt composition, a first for this type of modeling. As pointed out by Gaetani (2004), it is in predictive expressions for D_0 that the influence of melt composition and structure is most likely to be manifest. The revised model, consisting of this statistical D_0 expression combined with expressions for r_0 and E based on crystal-chemical considerations, accounts for trivalent partitioning as well as did the original WvW01 version when applied to the same datasets as was that original model. In addition, it successfully accounts for partitioning in more Fe-rich compositional systems, which the WvW01 model could not, and much more closely predicts partitioning in majorite-rich garnets. No terms expressly linked to majorite content were found to be statistically significant and additional data coverage is needed to make better predictions for majoritic garnets, although in the crystal-chemical E model (van Westrenen and Draper, this issue), there is explicit incorporation of a majorite component in the form of $(Al + Cr)_{apfu}$ [the number of atoms per formula unit (12 oxygen) of Al and Cr in garnet].

The new model fails badly, however, at predicting trivalent partitioning in hydrous systems, both for lower pressure, generally pyropic garnets like those produced by Nicholls and Harris (1980) and Barth et al. (2002), and majoritic garnet grown from a hydrous pyrolite composition by Inoue et al. (2000). In the following sections, we detail the choice of parameters used in the statistical evaluations, present the results of multiple linear regression analysis, and document their statistical significance. We then present the preferred model expressions at this stage of our work, show the degree to which the new preferred model accounts for a range of garnet-melt trivalent partitioning data, and outline gaps that remain to be filled. Finally, we show that partitioning of tetravalent cations (e.g. Zr, Hf, Ti) is not predictable at present using either lattice-strain or statistical formulations.

Approach and computations

In this section, we summarize the data sources used in our analysis, and outline the compositional variables chosen for statistical evaluation. We then present the calculations themselves and their results, showing which of the chosen variables can produce statistically defensible expressions for the lattice-strain parameters used in the predictive model. All statistical calculations presented here were performed using the statistical software package SPSS© version 15.0 for Windows.

Expanded database

Experimental data used in our modeling come from three categories of sources: those that were already available for inclusion in the original WvW01 model; those we have produced in studies intended in part for the specific purpose of expanding the compositional range available for WvW01; and those that have been published in the intervening years by other research groups. Table 1 lists these data sources along with the general range of compositions (basaltic, *sensu lato*, unless otherwise noted) and experimental conditions.

The data set listed in Table 1 is not identical to the one used in van Westrenen and Draper (this issue) for several reasons. First, Table 1 lists several garnet-melt partitioning experiments in hydrous systems, which were used to gauge the success of the statistical model in predicting hydrous D values. Our companion paper focuses exclusively on anhydrous experiments. Second, only data sets that include D values for scandium can produce best-fit values for D_0, r_0, and E simultaneously without making additional assumptions, such as those described in the following paragraph. Scandium's ionic radius of 0.87 Å for coordination number 8 (Shannon 1976) is lower than the r_0 values that result from garnet-melt partitioning data (van Westrenen et al. 1999). For natural garnets, r_0 values are typically 0.91–0.93 Å ; all the other trivalent cations that partition into garnet's X-site (Y, REE) have radii larger than this value. As a result, in the absence of Sc data the left-hand limbs of parabolae formed by plotting D values versus ionic radius are unconstrained. For example, consider three experiments from the studies listed in Table 1: run MP240 of Pertermann et al. (2004), run 16 of van Westrenen et al. (2000b), and runs 180 + 252 from Draper et al. (2003). Sc was included in these experiments and hence Eq. 1 yields values for D_0, r_0, and E. If D values for

Table 1 List of garnet-melt partitioning experimental studies used in this work

Reference	Conditions
Sc-bearing experiments incorporated in statistically-evaluated database	
Barth et al. (2002)	1.8 GPa, ~1,000°C, hydrous, eclogitic/tonalitic compositions
Bennett et al. (2004)	3 GPa, 1,300–1,400°C, anhydrous, CMAS with Na, Ti
Corgne and Wood (2004)	25 GPa, 2,300°C, anhydrous, majoritic garnet
Draper et al. (2003)	5–9 GPa, 1,750–1,950°C, anhydrous, majoritic garnet, Fe-rich
Draper et al. (2006)	2–7 GPa, 1,600–1,800°C, anhydrous, majoritic garnet, Fe-rich
Dwarzski et al. (2006)	5–7 GPa, 1,600–1,700°C, anhydrous, Fe-, Ti-rich
Hauri et al. (1994)	2.5 GPa, 1,430°C, anhydrous
Jenner et al. (1993)[a]	2.5 GPa, 1,000–1,100°C, hydrous
Kato et al. (1988)[a]	15–24 GPa, 2,100–2,260°C, anhydrous, majoritic garnet
Pertermann et al. (2004)	~3 GPa, 1,325–1,400°C, anhydrous, eclogitic composition
Sisson and Bacon (1992)	~1 GPa, 980°C, hydrous, rhyolitic composition
van Westrenen et al. (1999)	3 GPa, ~1,550°C, anhydrous, CMAS
van Westrenen et al. (2000b)	3 GPa, ~1,550°C, anhydrous, CMAS-Fe
Yurimoto and Ohtani (1992)	16–20 GPa, 1,900–2,000°C, anhydrous, majoritic garnet
Sc-absent experiments, not included in statistically-evaluated database	
Johnson (1994)	3 GPa, 1,430°C, anhydrous
Klein et al. (2000)	1–3 GPa, 900–1,150°C, hydrous, andesitic to tonalitic melts
Klemme et al. (2002)	3 GPa, 1,400°C, anhydrous
Nicholls and Harris (1980)	2–3 GPa, 940–1,420°C, dacitic melts, hydrous
Salters and Longhi (1999)	2.8 GPa, 1,500–1,550°C, anhydrous
Salters et al. (2002)	2.8–3.4 GPa, 1,465–1,660°C, anhydrous
Shimizu and Kushiro (1975)	3 GPa, 1,275°C, anhydrous
Walter et al. (2004)	~23 GPa, ~2,300°C, anhydrous, majoritic garnet

[a] Not all experiments in these studies included data for Sc, and hence not all were included in statistical database

Sc are omitted in those fits, i.e. using only the limbs of the parabolae at higher ionic radius values than expected r_0, drastically different and unrealistic results are obtained. For run MP240, the Sc-included fits yield values for D_0, E, and r_0 of 11.95 ± 2.41, 563 ± 54 GPa, and 0.914 ± 0.012 Å, respectively; the Sc-excluded values are 408 ± 726, 250 ± 76 GPa, and 0.711 ± 0.109 Å. For run 16, we have 6.20 ± 1.66, 406 ± 77 GPa, and 0.912 Å with Sc versus 491 ± 3,010, 127 ± 139 GPa, and 0.546 ± 0.577 Å without; and for 180 + 252, we have 2.51 ± 0.30, 480 ± 53 GPa, and 0.911 ± 0.010 Å versus 131 ± 265, 138 ± 57 GPa, and 0.578 ± 0.193 Å. Similar relationships were also described by van Westrenen et al. (2000b) (their Fig. 5 and p. 196).

Many garnet-melt partitioning studies did not include Sc (see Table 1). Using additional constraints, meaningful fits to Sc-absent data sets can still be obtained. For example, a predictive model for r_0 based on Sc-bearing data can be combined with Eq. 1 to obtain best-fit values for E and D_0 in Sc-absent experiments, e.g. van Westrenen et al. (2000b). These values can then be used to construct predictive models for E and D_0. Although we consider this a perfectly valid approach for the crystal-chemical and thermodynamic models of van Westrenen and Draper (this issue), this could introduce artificial bias into our statistical evaluations. Therefore, only Sc-bearing experiments for which physically-realistic results for D_0, r_0, and E can be precisely determined simultaneously were included in our statistical analyses.

Finally, although van Westrenen and Draper (this issue) opted to omit data from some earlier studies on partitioning in majoritic garnet, e.g. Kato et al. (1988) and Yurimoto and Ohtani (1992), we chose to include data from Sc-bearing experiments from those two studies in our statistical analysis largely because no other data were available at pressures from ~16 to 20 GPa for majoritic garnets. As we show below, our revised models nevertheless significantly improve predicted D values for such studies.

For these experiments, fitting the data to Eq. 1 yields values for D_0, r_0, and E for each experiment; we refer to these three values as the *lattice-strain fit parameters*. We then selected 16 variables intended to reflect garnet or liquid composition, garnet crystal chemistry, melt structure, temperature, and pressure; we refer to these simply as *variables*. Possible correlations between these variables were first assessed to find combinations in which all variables were independent of one another. Then, each individual lattice-strain fit parameter (D_0 r_0, and E) was

multiply regressed against combinations of these independent variables using both standard and "stepwise" approaches. Multiple linear regression results for these permutations show which are robust predictors and which are not.

Choosing variables for statistical evaluations

The 16 specific variables used in our statistical calculations, listed in Table 2, were chosen to reflect the potential influence of intensive and extensive parameters on garnet-melt partitioning. Variables expressing garnet compositional variation include contents of the endmember components pyrope (Py), grossular (Gro), and almandine (Alm), calculated from electron microprobe determinations of the major-element compositions of garnets grown in the experiments. Variables chosen to express the transition from "normal" garnet to higher-pressure, majoritic garnet are the stoichiometric values of silicon and aluminum per 12-oxygen formula unit; with increasing majorite content, Si increases from the canonical 3.0 atoms per formula unit (apfu) typical of lower pressure, pyropic garnets, while Al decreases from the canonical 2.0 apfu. These changes reflect the enhanced solubility with increasing pressure of a pyroxene component, $R_2^{2+}Si_2O_6$, in the Y-site of garnet, $R_3^{2+}R_2^{3+}[SiO_4]_3$, via the substitution $^{VI}[R^{2+} + Si^{4+}] = 2^{VI}R^{3+}$ (Xirouchakis et al. 2002; Draper et al. 2003); this change can be envisioned as a solid solution between pyrope and enstatite. Variables chosen to address garnet-melt major element equilibrium include D values for Ca, Mg, and Fe (the major constituent cations for the garnet X-site) and K_D values for both Fe–Mg and Al–Si exchange, i.e. $K_D^{Fe-Mg} = \frac{FeO^{gt}MgO^{liq}}{FeO^{liq}MgO^{gt}}$; $K_D^{Al-Si} = \frac{Al_2O_3^{gt}SiO_2^{liq}}{Al_2O_3^{liq}SiO_2^{gt}}$ where gt and liq refer to contents in coexisting garnet and liquid, respectively. Melt composition is addressed using melt FeO/SiO_2, MgO/SiO_2, and Mg# [molar Mg/(Mg + Fe)]. Melt structure is represented by the variables NBO/t, the ratio of non-bridging oxygens to tetrahedrally coordinated cations in a liquid composition (Mysen 1983), and ionic porosity, a measure of the "empty space" in a silicate melt (Dowty 1980; Fortier and Giletti 1989; Carroll and Draper 1994). Although the data set (Table 1) contains several garnet-hydrous melt partitioning experiments, H_2O was not included as a parameter in our statistical assessments. This is because only seven experimental runs in extant studies measuring garnet partitioning under hydrous conditions included Sc in the suite of analyte elements (Jenner et al. 1993; Barth et al. 2002). As discussed above, inclusion of Sc is essential for assessing all three lattice-strain fit parameters simultaneously. Again, it would be possible to constrain D_0 values from r_0 and E models based on Sc-bearing experiments, as was done by Wood and Blundy (2002) in their attempt to quantify the effect of H_2O on garnet-melt partitioning. However, doing so introduces an additional level of model-dependence, which we were eager to avoid. In short, the currently available data for garnet-melt partitioning in hydrous systems are insufficient to include H_2O as a variable for statistical evaluation, and such experiments should clearly be a focus for future work.

Table 2 Variables chosen for possible use in statistical regressions

Quantity	Description
D_{Ca}, D_{Mg}, D_{Fe}	Garnet-liquid D values for major constituents of X-site
K_D for Fe–Mg, Al–Si	$K_D^{Fe-Mg} = \frac{FeO^{gt}MgO^{liq}}{FeO^{liq}MgO^{gt}}$; $K_D^{Al-Si} = \frac{Al_2O_3^{gt}SiO_2^{liq}}{Al_2O_3^{liq}SiO_2^{gt}}$
Gr, Py, Alm	Mol% grossular, pyrope, almandine in garnet
Si, Al per formula unit (pfu)	Number Si and Al cations per 12-oxygen formula unit
Melt Mg#	Molar Mg/Mg + Fe in melt
Melt MgO/SiO_2	Ratio of wt% oxide MgO to SiO_2 in melt
Melt FeO/SiO_2	Ratio of wt% oxide FeO to SiO_2 in melt
Melt NBO/t	Ratio of non-bridging oxygens to tetrahedral cations in melt (Mysen 1983)
Melt ionic porosity	Measure of melt "empty space"; Dowty (1980), Carroll and Draper (1994)
Temperature	
Pressure	

Assessing bivariate correlations among variables

Before using any of the variables chosen for statistical analysis, it must be demonstrated that they are not correlated with one another; only independent variables should be used in predicting garnet-melt partitioning. We accomplished this by computing correlation matrices consisting of Pearson's correlation coefficients for all possible variable pairs with their associated p-values. The p-values (two-tailed) denote the statistical significance of the correlation coefficients; at the 95% confidence limit, those correlations with p-values less than or equal to 0.05 are considered significant, whereas those with p-values greater than 0.05 are not. We computed correlation matrices for two versions of the dataset. The first includes every experiment from the Sc-bearing studies listed in Table 1. The second excludes the data from the seven Sc-bearing experiments that were performed under hydrous conditions (Jenner et al. 1993; Barth et al. 2002); recall that the hydrous experiments of Nicholls and Harris (1980) and Klein et al. (2000) lacked Sc and so cannot be fitted to Eq. 1. We proceeded in this fashion because the hydrous experiments were run at hundreds of degrees cooler temperatures than all the other experiments, which may result in discontinu-

Table 3 Matrix showing correlations between variables chosen for statistical analysis; data from hydrous experiments included

	10,000/T	P (GPa)	Fe–Mg K_D	Al–Si K_D	FeO/SiO_2	MgO/SiO_2	Mg#	Ionic Porosity	NBO/t	Mol% Gr	Mol% Py	Mol% Alm	D_{Mg}	D_{Ca}	D_{Fe}	Si per 12 Oxy	Al per 12 Oxy
10,000/T		–0.759	**–0.021**	**–0.278**	**–0.272**	–0.844	–0.501	–0.783	–0.827	0.585	–0.728	0.521	0.737	0.808	0.824	–0.758	0.731
		0.000	**0.889**	**0.061**	**0.067**	0.000	0.000	0.000	0.000	0.000	0.000	0.000	0.000	0.000	0.000	0.000	0.000
P (GPa)	–0.759		**0.007**	**0.085**	**0.048**	0.760	0.442	0.694	0.628	–0.532	0.669	–0.470	–0.365	–0.363	–0.460	0.921	–0.899
	0.000		**0.965**	**0.573**	**0.749**	0.000	0.002	0.000	0.000	0.000	0.000	0.001	0.013	0.013	0.003	0.000	0.000
Fe–Mg K_D	**–0.021**	**0.007**		**–0.286**	–0.353	**0.256**	**0.282**	**–0.135**	**0.098**	**0.095**	**0.015**	**–0.110**	**–0.224**	**0.092**	**0.131**	**0.113**	**–0.085**
	0.889	**0.965**		**0.054**	0.016	**0.086**	**0.057**	**0.372**	**0.515**	**0.530**	**0.922**	**0.468**	**0.135**	**0.542**	**0.421**	**0.456**	**0.572**
Al–Si K_D	**–0.278**	**0.085**	**–0.286**		0.817	**0.251**	**–0.269**	0.643	0.516	–0.597	**0.082**	**0.258**	**–0.204**	**–0.281**	–0.344	**0.084**	–0.309
	0.061	**0.573**	**0.054**		0.000	**0.092**	**0.070**	0.000	0.000	0.000	**0.587**	**0.083**	**0.174**	**0.059**	0.030	**0.578**	0.037
FeO/SiO_2	**–0.272**	**0.048**	–0.353	0.817		**0.202**	–0.474	0.571	0.483	–0.609	**–0.081**	0.450	–0.328	**–0.290**	–0.486	**0.064**	–0.314
	0.067	**0.749**	0.016	0.000		**0.178**	0.001	0.000	0.001	0.000	**0.592**	0.002	0.026	**0.051**	0.001	**0.670**	0.034
MgO/SiO_2	–0.844	0.760	**0.256**	**0.251**	**0.202**		0.558	0.801	0.921	–0.694	0.822	–0.551	–0.584	–0.620	–0.637	0.867	–0.857
	0.000	0.000	**0.086**	**0.092**	**0.178**		0.000	0.000	0.000	0.000	0.000	0.000	0.000	0.000	0.000	0.000	0.000
Mg#	–0.501	0.442	**0.282**	**–0.269**	–0.474	0.558		**0.234**	0.344	**–0.001**	0.795	–0.968	–0.341	–0.508	–0.352	0.500	–0.306
	0.000	0.002	**0.057**	**0.070**	0.001	0.000		**0.117**	0.019	**0.995**	0.000	0.000	0.020	0.000	0.026	0.000	0.038
Ionic porosity	–0.783	0.694	**–0.135**	0.643	0.571	0.801	**0.234**		0.891	–0.880	0.670	**–0.256**	–0.481	–0.624	–0.674	0.698	–0.794
	0.000	0.000	**0.372**	0.000	0.000	0.000	**0.117**		0.000	0.000	0.000	**0.086**	0.001	0.000	0.000	0.000	0.000
NBO/t	–0.827	0.628	**0.098**	0.516	0.483	0.921	0.344	0.891		–0.788	0.694	–0.336	–0.648	–0.704	–0.752	0.716	–0.776
	0.000	0.000	**0.515**	0.000	0.001	0.000	0.019	0.000		0.000	0.000	0.022	0.000	0.000	0.000	0.000	0.000
Mol% Gr	0.585	–0.532	**0.095**	–0.597	–0.609	–0.694	**–0.001**	–0.880	–0.788		–0.524	**0.017**	0.307	0.434	0.557	–0.540	0.707
	0.000	0.000	**0.530**	0.000	0.000	0.000	**0.995**	0.000	0.000		0.000	**0.913**	0.038	0.003	0.000	0.000	0.000
Mol% Py	–0.728	0.669	**0.015**	**0.082**	**–0.081**	0.822	0.795	0.670	0.694	–0.524		–0.843	–0.342	–0.652	–0.482	0.743	–0.621
	0.000	0.000	**0.922**	**0.587**	**0.592**	0.000	0.000	0.000	0.000	0.000		0.000	0.020	0.000	0.002	0.000	0.000
Mol% Alm	0.521	–0.470	**–0.110**	**0.258**	0.450	–0.551	–0.968	**–0.256**	–0.336	**0.017**	–0.843		**0.249**	0.514	0.353	–0.529	0.318
	0.000	0.001	**0.468**	**0.083**	0.002	0.000	0.000	**0.086**	0.022	**0.913**	0.000		**0.095**	0.000	0.025	0.000	0.031
D_{Mg}	0.737	–0.365	**–0.224**	**–0.204**	–0.328	–0.584	–0.341	–0.481	–0.648	0.307	–0.342	**0.249**		0.769	0.855	–0.397	0.396
	0.000	0.013	**0.135**	**0.174**	0.026	0.000	0.020	0.001	0.000	0.038	0.020	**0.095**		0.000	0.000	0.006	0.006
D_{Ca}	0.808	–0.363	**0.092**	**–0.281**	**–0.290**	–0.620	–0.508	–0.624	–0.704	0.434	–0.652	0.514	0.769		0.909	–0.391	0.334
	0.000	0.013	**0.542**	**0.059**	**0.051**	0.000	0.000	0.000	0.000	0.003	0.000	0.000	0.000		0.000	0.007	0.023
D_{Fe}	0.824	–0.460	**0.131**	–0.344	–0.486	–0.637	–0.352	–0.674	–0.752	0.557	–0.482	0.353	0.855	0.909		–0.446	0.488
	0.000	0.003	**0.421**	0.030	0.001	0.000	0.026	0.000	0.000	0.000	0.002	0.025	0.000	0.000		0.004	0.001
Si per 12 O	–0.758	0.921	**0.113**	**0.084**	**0.064**	0.867	0.500	0.698	0.716	–0.540	0.743	–0.529	–0.397	–0.391	–0.446		–0.922
	0.000	0.000	**0.456**	**0.578**	**0.670**	0.000	0.000	0.000	0.000	0.000	0.000	0.000	0.006	0.007	0.004		0.000

Table 3 continued

	10,000/T	P (GPa)	Fe–Mg K_D	Al–Si K_D	FeO/SiO_2	MgO/SiO_2	Mg#	Ionic Porosity	NBO/t	Mol% Gr	Mol% Py	Mol% Alm	D_{Mg}	D_{Ca}	D_{Fe}	Si per 12 Oxy	Al per 12 Oxy
Al per 12 O	0.731	–0.899	**–0.085**	–0.309	–0.314	–0.857	–0.306	–0.794	–0.776	0.707	–0.621	0.318	0.396	0.334	0.488	–0.922	
	0.000	0.000	**0.572**	0.037	0.034	0.000	0.038	0.000	0.000	0.000	0.000	0.031	0.006	0.023	0.001	0.000	

Upper line for each entry is the Pearson correlation coefficient; lower line is p-value for significance of correlation (2-tailed). Variable pairs having $p < 0.05$ are correlated at 95% confidence. Tabulated p values of 0.000 signify $p < 0.0001$. Entries in boldface denote variable pairs that do not show significant correlations with one another and are thus suitable for further statistical analyses

ities in some variables, and because the role of water in affecting partitioning in general is still poorly understood.

Tables 3 and 4 give the correlation matrices for these two cases. Each entry in these tables consists of the Pearson coefficient (upper line) and two-tailed significance (lower line) for each possible variable pair. Entries for which correlations are not significant ($p > 0.05$) are denoted in boldface type. In both sets of results, the garnet-melt exchange coefficients for Fe–Mg and for Al–Si are the least correlated with the others; some variables (e.g. D_{Fe}) are significantly correlated with almost all of the other chosen variables. From these two tables, subsets of variables can be chosen that contain only variables that are linearly independent of one another. For the assessment that included the hydrous-experiment data, fourteen such subsets can be identified; for the hydrous-excluded assessment, 15 subsets can be used. Some of the subsets are common to both groups, whereas others appear in only one group (these will be presented below). Our next step was therefore to perform multiple linear regressions on each of these subsets to determine whether any of them usefully predict any of the lattice-strain fit parameters D_0, r_0, and E.

Multiple linear regressions

Multiple linear regressions were performed on each subset of independent variables in two ways. In the first, all variables in the subset were included in the regression. In the second, three "stepwise" techniques were employed. The use of the stepwise approach to augment the standard technique allows us to determine if all variables in the regression are truly required. All approaches use an F statistic and its associated significance to assess the contributions from each variable in a regression. The significance (p-value) is defined in the same way as for the correlation matrices described above. In the traditional stepwise technique, at each step the independent variable not in the equation that has the smallest significance of F is entered into the regression, if that significance is sufficiently small. Variables already in the regression equation are removed if their significance of F becomes sufficiently large. The method terminates when no more variables are eligible for inclusion or removal. The threshold significance values used for inclusion or removal were 0.05 and 0.10, respectively.

Two additional stepwise techniques were also employed. The first is *backward elimination*, a variable selection procedure in which all variables are entered into the equation and then sequentially removed. The variable with the smallest partial correlation with the dependent variable is considered first for removal, which occurs if it meets the criterion for elimination. After the first variable

Table 4 Matrix showing correlations between variables chosen for statistical analysis; data from hydrous experiments omitted

	10,000/T	P (GPa)	Fe–Mg K_D	Al–Si K_D	FeO/SiO_2	MgO/SiO_2	Mg#	Ionic Porosity	NBO/t	Mol% Gr	Mol% Py	Mol% Alm	D_{Mg}	D_{Ca}	D_{Fe}	Si per 12 Oxy	Al per 12 Oxy
10,000/T		–0.870	**–0.082**	**–0.255**	**–0.207**	–0.900	–0.434	–0.859	–0.847	0.699	–0.799	0.455	0.756	0.576	0.807	–0.876	0.873
		0.000	**0.621**	**0.117**	**0.206**	0.000	0.006	0.000	0.000	0.000	0.000	0.004	0.000	0.000	0.000	0.000	0.000
P (GPa)	–0.870		**0.017**	**0.038**	**0.005**	0.735	0.387	0.662	0.588	–0.511	0.663	–0.423	–0.444	**–0.264**	–0.501	0.917	–0.893
	0.000		**0.917**	**0.820**	**0.976**	0.000	0.015	0.000	0.000	0.001	0.000	0.007	0.005	**0.104**	0.003	0.000	0.000
Fe–Mg K_D	**–0.082**	**0.017**		**–0.289**	–0.382	**0.309**	0.332	**–0.124**	**0.126**	**0.065**	**0.098**	**–0.192**	**–0.260**	**0.077**	**0.181**	**0.130**	**–0.093**
	0.621	**0.917**		**0.074**	0.016	**0.055**	0.039	**0.453**	**0.444**	**0.695**	**0.553**	**0.242**	**0.110**	**0.640**	**0.313**	**0.431**	**0.572**
Al–Si K_D	**–0.255**	**0.038**	**–0.289**		0.840	**0.205**	–0.371	0.632	0.510	–0.582	**0.001**	0.382	**–0.282**	**–0.282**	–0.452	**0.033**	**–0.278**
	0.117	**0.820**	**0.074**		0.000	**0.211**	0.020	0.000	0.001	0.000	**0.997**	0.016	**0.078**	**0.082**	0.008	**0.841**	**0.086**
FeO/SiO_2	**–0.207**	**0.005**	–0.382	0.840		**0.151**	–0.561	0.585	0.456	–0.627	**–0.122**	0.544	**–0.314**	**–0.212**	–0.467	**0.032**	**–0.297**
	0.206	**0.976**	0.016	0.000		**0.359**	0.000	0.000	0.004	0.000	**0.459**	0.000	**0.052**	**0.195**	0.006	**0.849**	**0.066**
MgO/SiO_2	–0.900	0.735	**0.309**	**0.205**	**0.151**		0.500	0.773	0.908	–0.694	0.834	–0.495	–0.775	–0.556	–0.728	0.861	–0.858
	0.000	0.000	**0.055**	**0.211**	**0.359**		0.001	0.000	0.000	0.000	0.000	0.001	0.000	0.000	0.000	0.000	0.000
Mg#	–0.434	0.387	0.332	–0.371	–0.561	0.500		**0.116**	**0.256**	**0.088**	0.773	–0.975	–0.468	–0.511	–0.518	0.439	**–0.247**
	0.006	0.015	0.039	0.020	0.000	0.001		**0.480**	**0.116**	**0.596**	0.000	0.000	0.003	0.001	0.002	0.005	**0.130**
Ionic porosity	–0.859	0.662	**–0.124**	0.632	0.585	0.773	**0.116**		0.894	–0.889	0.629	**–0.125**	–0.731	–0.641	–0.898	0.667	–0.782
	0.000	0.000	**0.453**	0.000	0.000	0.000	**0.480**		0.000	0.000	0.000	**0.447**	0.000	0.000	0.000	0.000	0.000
NBO/t	–0.847	0.588	**0.126**	0.510	0.456	0.908	**0.256**	0.894		–0.816	0.699	**–0.249**	–0.810	–0.651	–0.844	0.698	–0.775
	0.000	0.000	**0.444**	0.001	0.004	0.000	**0.116**	0.000		0.000	0.000	**0.126**	0.000	0.000	0.000	0.000	0.000
Mol% Gr	0.699	–0.511	**0.065**	–0.582	–0.627	–0.694	**0.088**	–0.889	–0.816		–0.487	**–0.096**	**0.583**	0.496	0.805	–0.517	0.703
	0.000	0.001	**0.695**	0.000	0.000	0.000	**0.596**	0.000	0.000		0.002	**0.561**	**0.000**	0.001	0.000	0.001	0.000
Mol% Py	–0.799	0.663	**0.098**	**0.001**	**–0.122**	0.834	0.773	0.629	0.699	–0.487		–0.803	–0.681	–0.740	–0.765	0.739	–0.624
	0.000	0.000	**0.553**	**0.997**	**0.459**	0.000	0.000	0.000	0.000	0.002		0.000	0.000	0.000	0.000	0.000	0.000
Mol% Alm	0.455	–0.423	**–0.192**	0.382	0.544	–0.495	–0.975	**–0.125**	**–0.249**	**–0.096**	–0.803		0.417	0.507	0.546	–0.479	**0.265**
	0.004	0.007	**0.242**	0.016	0.000	0.001	0.000	**0.447**	**0.126**	**0.561**	0.000		0.008	0.001	0.001	0.002	**0.104**
D_{Mg}	0.756	–0.444	**–0.260**	**–0.282**	**–0.314**	–0.775	–0.468	–0.731	–0.810	**0.583**	–0.681	0.417		0.788	0.904	–0.552	0.562
	0.000	0.005	**0.110**	**0.078**	**0.052**	0.000	0.003	0.000	0.000	**0.000**	0.000	0.008		0.000	0.000	0.000	0.000
D_{Ca}	0.576	**–0.264**	**0.077**	**–0.282**	**–0.212**	–0.556	–0.511	–0.641	–0.651	0.496	–0.740	0.507	0.788		0.885	–0.329	**0.273**
	0.000	**0.104**	**0.640**	**0.082**	**0.195**	0.000	0.001	0.000	0.000	0.001	0.000	0.001	0.000		0.000	0.041	**0.092**
D_{Fe}	0.807	–0.501	**0.181**	–0.452	–0.467	–0.728	–0.518	–0.898	–0.844	0.805	–0.765	0.546	0.904	0.885		–0.556	0.598
	0.000	0.003	**0.313**	0.008	0.006	0.000	0.002	0.000	0.000	0.000	0.000	0.001	0.000	0.000		0.001	0.000
Si per 12 O	–0.876	0.917	**0.130**	**0.033**	**0.032**	0.861	0.439	0.667	0.698	–0.517	0.739	–0.479	–0.552	–0.329	–0.556		–0.923
	0.000	0.000	**0.431**	**0.841**	**0.849**	0.000	0.005	0.000	0.000	0.001	0.000	0.002	0.000	0.041	0.001		0.000
Al per 12 O	0.873	–0.893	**–0.093**	**–0.278**	**–0.297**	–0.858	**–0.247**	–0.782	–0.775	0.703	–0.624	**0.265**	0.562	**0.273**	0.598	–0.923	
	0.000	0.000	**0.572**	**0.086**	**0.066**	0.000	**0.130**	0.000	0.000	0.000	0.000	**0.104**	0.000	**0.092**	0.000	0.000	

Details as in Table 3

is removed, the variable remaining in the equation with the smallest partial correlation is considered next. The procedure stops when there are no variables in the equation that satisfy the removal criteria. The second additional technique, *forward selection*, is a selection procedure in which variables are sequentially entered into the model. The first variable considered for entry into the equation is the one with the largest positive or negative correlation with the dependent variable. This variable is entered into the equation only if it satisfies the criterion for entry. If the first variable is entered, the independent variable not in the equation that has the largest partial correlation is considered next. The procedure stops when there are no variables that meet the entry criterion. In both these latter techniques, the same criteria for entry and removal were used, namely significance of F of 0.05 and 0.10, respectively. In most cases, the results of the three stepwise techniques yield identical conclusions regarding which variables are required and which can be eliminated.

After performing these four types of multiple linear regression on each of the variable subsets identified using the bivariate correlation procedure, for each of the three lattice-strain fit parameters, we find that for E and r_0 none of the regressions produced useful predictive expressions. In all cases for those two parameters, multiple correlation coefficients (R) were well below 0.5 with coefficients of determination (R^2) below 0.25. Plots of predicted versus measured values of E and r_0 from these regressions produce "shotgun" patterns instead of anything resembling one-to-one trends. This lack of correlation is likely due to the rather more complicated formulations and manipulations required to produce the crystal-chemical expressions that do produce useful predictors for these two quantities (van Westrenen and Draper, this issue). Clearly there are nonlinear components to these relationships, and these do not manifest themselves in the multiple-linear correlations tested in this analysis. We therefore conclude that at present, available garnet-melt and majorite-melt partitioning data cannot be used to define statistically-significant predictive relationships for these lattice-strain parameters of the type tested for here. That no statistical models could be found for r_0 shows, in our view, that it is essential to base r_0 models on systematic experiments in simple systems, as discussed previously in Van Westrenen et al. (1999, 2000a, b). The crystal-chemical r_0 model of Van Westrenen and Draper (this issue) was obtained in a stepwise approach, building upon these simple system experiments to derive crystal-chemistry effects prior to deriving pressure and temperature terms.

In contrast, correlation coefficients and coefficients of determination for models of D_0 indicate potentially useful predictive expressions. Multiple linear regression results for the D_0 expressions are summarized in Table 5. This table lists the variable subsets that we determined to be linearly independent of one another using the bivariate correlation calculations presented above. For each of the two versions of the dataset (one including the few hydrous experiments, the other excluding them), we tabulate R^2 values for the four types of regression computed for each of these subsets. For the hydrous-included data, the best result is for an expression containing Fe–Mg K_D, Al–Si K_D, D_{Mg}, and garnet mol% almandine, with an R^2 value of 0.731. However, an even stronger result emerges from the regressions performed on the hydrous-excluded data. As shown from bivariate correlation results given in Table 4, mol% almandine cannot be used in combination with Fe–Mg K_D, Al–Si K_D, and D_{Mg} in this case, because it shows a correlation with Al–Si K_D with a significance <0.05. The results for the three remaining independent variables give an R^2 of 0.867 (boldface entry in Table 5). Below, we examine this result in more detail.

Successful D_0 model

The apparently successful model listed in boldface in Table 5 relates D_0 to the variable subset Fe–Mg K_D, Al–Si K_D, and D_{Mg}. The R^2 values for this subset for all four methods of regression are identical at 0.867. Part of the output for these regressions is a t-statistic for each of the coefficients determined by the regression and its significance (p-value). As in the computations above, p-values less than 0.05 connote statistical significance for the regression coefficients, whereas values above that threshold signify non-significance. When all three variables are included in the regression, the significance of the t-statistic associated with the coefficient for Al–Si K_D is 0.722, greatly in excess of the threshold value of 0.05. Furthermore, in each of the three stepwise methods, that variable is excluded by the regression procedure as not being truly required in the regression. Finally, the three stepwise regression procedures also give identical results for the regression coefficients and significance values for the two surviving variables, Fe–Mg K_D and D_{Mg}, as well as for the F statistic associated with the overall regression result. From these results, it is clear that Al–Si K_D is not in fact required in predicting D_0.

The resulting expression for predicting D_0 (Table 6) is 3.24 ± 1.46 (Fe–Mg K_D) + 3.01 ± 0.20 (D_{Mg}) – 2.59 ± 1.04 (errors are 1σ) The WvW01 model also included a D_{Mg} term. The addition of the Fe–Mg exchange term represents an additional effect of melt composition on predicted D_0 that was hitherto not identified. In Fig. 2a we plot the predicted D_0 values against those from fits of the experimental data to Eq. 1; compare to Fig. 9 in van Westrenen and Draper (this issue). The three outlying points at high

Table 5 Coefficients of determination (= square of multiple correlation coefficients) for multiple linear regressions performed on subsets of variables

	All variables	Stepwise	Backward	Forward
Regression subsets from datablock analyzed *including* results from hydrous experiments				
10,000/T, Fe–Mg K_D, Al–Si K_D, melt FeO/SiO_2	0.706	0.691	0.691	0.691
10,000/T, Fe–Mg K_D, Al–Si K_D	0.682	0.651	0.674	0.651
P (GPa), Fe–Mg K_D, Al–Si K_D, melt FeO/SiO_2	0.471	0.429	0.470	0.429
P (GPa), Fe–Mg K_D, Al–Si K_D	0.409	0.385	0.385	0.385
Fe–Mg K_D, Al–Si K_D, melt MgO/SiO_2	0.577	0.536	0.572	0.536
Fe–Mg K_D, Al–Si K_D, garnet mol% Alm, D_{Mg}	0.731	0.731	0.731	0.731
Fe–Mg K_D, Al–Si K_D, melt Mg#	0.489	0.487	0.487	0.487
Fe–Mg K_D, Al–Si K_D, garnet mol% Py	0.520	0.498	0.498	0.498
Fe–Mg K_D, Al–Si K_D, garnet mol% Alm	0.463	0.441	0.441	0.441
Fe–Mg K_D, Al–Si K_D, D_{Mg}	0.609	0.608	0.608	0.608
Fe–Mg K_D, Al–Si K_D, D_{Ca}	0.698	0.642	0.698	0.642
Fe–Mg K_D, melt ionic porosity, melt Mg#	0.641	0.637	0.637	0.637
Fe–Mg K_D, garnet mol% Gr, melt Mg#	0.555	0.555	0.555	0.555
Fe–Mg K_D, Al–Si K_D, Si per 12 oxygens	0.409	0.400	0.400	0.400
Regression subsets from datablock analyzed *excluding* results from hydrous experiments				
10,000/T, Fe–Mg K_D, Al–Si K_D	0.631	0.586	0.631	0.586
P (GPa), Fe–Mg K_D, Al–Si K_D	0.416	0.371	0.416	0.371
P (GPa), melt FeO/SiO_2, D_{Ca}	0.696	0.696	0.696	0.696
Fe–Mg K_D, Al–Si K_D, melt MgO/SiO_2	0.549	0.548	0.548	0.548
Fe–Mg K_D, Al–Si K_D, D_{Mg}	**0.867**	**0.867**	**0.867**	**0.867**
Fe–Mg K_D, melt ionic porosity, garnet mol% Alm	0.680	0.659	0.659	0.659
Fe–Mg K_D, melt NBO/t, garnet mol% Alm	0.608	0.608	0.608	0.608
Fe–Mg K_D, Al–Si K_D, Al per 12 oxygens	0.416	0.353	0.353	0.353
Fe–Mg K_D, Al–Si K_D, Si per 12 oxygens	0.422	0.399	0.399	0.399
Fe–Mg K_D, Al–Si K_D, D_{Ca}, Al per 12 oxygens	0.737	0.707	0.737	0.707
Fe–Mg K_D, D_{Ca}, Al per 12 oxygens	0.721	0.707	0.707	0.707
Fe–Mg K_D, Al–Si K_D, D_{Ca}	0.619	0.54	0.619	0.54
Al–Si K_D, D_{Ca}, Al per 12 oxygens	0.714	0.707	0.707	0.707
D_{Ca}, Al per 12 oxygens, melt FeO/SiO_2	0.722	0.707	0.707	0.707

See text for discussion. All abbreviations as in Table 2. Most successful multiple linear regression indicated with boldface; details of that model given in Table 6

predicted D_0 are the three Sc-bearing hydrous experiments of Barth et al. (2002), suggesting the model will not reliably predict partitioning in hydrous systems; we return to this point more fully below. A final indication that the variable Al–Si K_D is not required to predict D_0 is that if the regression coefficients including that variable are used, the positions of the plotted points are virtually indistinguishable from those on Fig. 2. That is, removal of that variable results in the same predicted D_0 values as when it is included. In Fig. 2b, we compare the D_0 values predicted by the thermodynamic and statistical approaches to fitted values for the subset of data for which this direct comparison is possible (see above and van Westrenen and Draper, this issue, for these constraints). Here it is evident that the two models predict D_0 equally well. There are no obvious conditions or compositions over which one model more successfully predicts D_0 than does the other, for

Table 6 Details of successful statistical D_0 model

Variable	Coefficient	t Statistic	P value
Fe–Mg K_D	3.24 ± 1.46	2.22	0.033
D_{Mg}	3.01 ± 0.20	15.19	<0.001
Intercept	–2.59 ± 1.04	–2.48	0.018

Abbreviations as in Table 2. Multiple regression coefficient (R) = 0.931; coefficient of determination (R^2) = 0.867. Model F value = 117 with significance <0.001

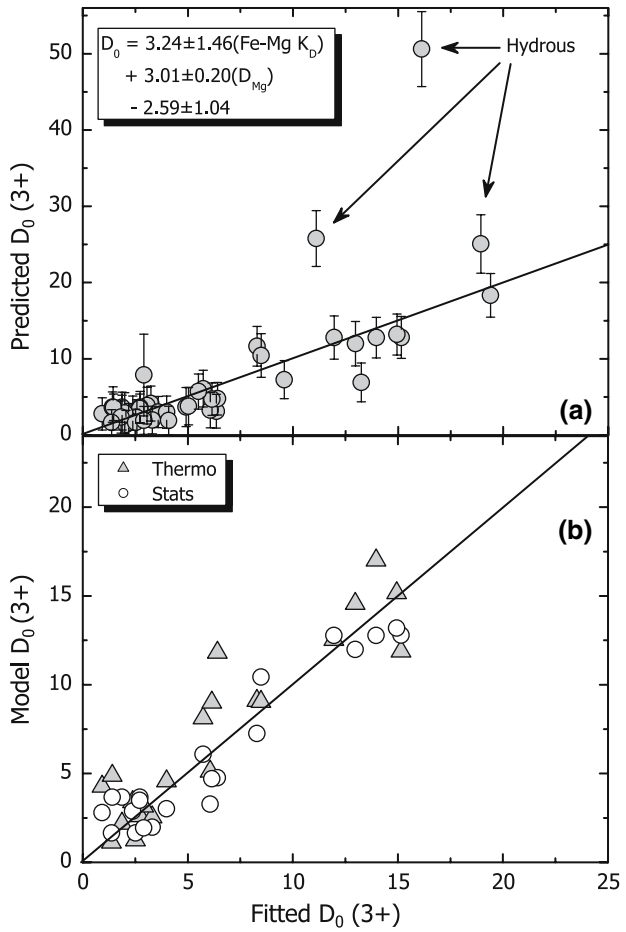

Fig. 2 **a** Plot of D_0 fitted to Eq. 1 from Sc-bearing experimental datasets versus D_0 predicted from multiple linear regressions (Tables 6, 7). Line illustrates one-to-one correspondence. Compare with Fig. 9 of van Westrenen and Draper (this issue). **b** Comparison of D_0 predicted from thermodynamic (*Thermo* in legend) and statistical (*Stats* in legend) models to D_0 fitted to Eq. 1 from Sc-bearing experimental datasets (error bars omitted); direct comparisons possible for only ~25 experiments because of constraints on data useable in the two approaches as described in these two companion papers. Statistical D_0 expression yields predictions as good as thermodynamic expression, although uncertainties are slightly greater. See text for discussion

example at one range of temperature or pressure or over a particular compositional range.

Updated model and comparisons

New model equations

Our updated predictive model now consists of new expressions for E, r_0, and D_0. The former two were derived in the first paper of this companion pair, and prediction of D_0 is possible using either the thermodynamic formulation in that paper or the statistical evaluations outlined here. The four expressions are written out in full in Table 7. An Excel spreadsheet set up to yield values for E, r_0, and D_0 from the relevant parameters, and to calculate through Eq. 1 predicted values for garnet-melt D values for the REE, Y and Sc, is available both by request from the authors and at the websites http://www.unm.edu/~draper/geo.html and http://www.geo.vu.nl/~wvwest/.

The crystal-chemical expression for r_0 has only very small uncertainties associated with the pressure and temperature terms, derived from mineral physics data on variations of the dimensions of the garnet X-site as a function of pressure, and from linear regression of pressure-corrected r_0 values against temperature, that when propagated result in uncertainties on r_0 of 0.01–0.001 Å, compared to typical absolute values of 0.88–0.99 Å. Model E values incorporate propagated uncertainties in r_0, in addition to errors in best-fit parameters associated with pressure, temperature, and majorite content terms (Table 7). Thus model E values are uncertain to within approximately 80 GPa out of 465–730 GPa typical of the garnet X-site. Propagation of the uncertainties in the statistical D_0 expression yields estimates that have uncertainties of approximately 20% relative, illustrated by the error bars on Fig. 2. We demonstrate below that the updated model, using the nominal predicted D_0 values, performs very well for all but hydrous compositional systems.

Users of this predictive model should be aware that they can choose between either the statistical or thermodynamic D_0 expressions. Advantages of the statistical D_0 expression include its simplicity (relying on fewer parameters) and its more explicit incorporation of the melt-compositional effect on predicted D values. Accordingly, use of the statis-

Table 7 Preferred predictive expressions

Equation 3 of van Westrenen et al. (this issue):

$r_0 =$ 0.9302 Py + 0.993 Gr + 0.916 Alm + 0.946 Spes + 1.05 (And + Uv) – 0.0044(±3) $(P - 3)$ + 0.000058(±7) $(T - 1817)$ [±least significant unit]

Equation 6 of van Westrenen and Draper (this issue):

$E =$ 2,826(±174) $(1.38 + r_0)^{-3}$ + 12.4(±13) (P) – 0.072(±7) (T) + 237(±8) $(\mathrm{Al} + \mathrm{Cr})_{\mathrm{apfu}}$

Thermodynamic D_0:

Equation 18 of van Westrenen et al. (this issue):

$$D_0(\mathrm{REE}) = \exp\left(\frac{400{,}290(\pm 1{,}100) + 4{,}586(\pm 150)P - 218(\pm 7)T}{RT}\right) \Big/ \left(\gamma_{\mathrm{Fe}}^{\mathrm{garnet}} D_{\mathrm{Fe}}\right)^2$$

Statistical D_0:

$D_0 =$ (3.24 ± 1.46) Fe–Mg K_D + (3.01 ± 0.20) D_{Mg} – (2.59 ± 1.04)

Abbreviations as in Table 2, with Spes, And, Uv = mol % spessartine, andradite, uvovarite respectively; $(\mathrm{Al} + \mathrm{Cr})_{\mathrm{apfu}}$ = Al and Cr cations per 12-oxygen formula unit; $D_{\mathrm{Fe}} = \mathrm{FeO}^{\mathrm{garnet}}/\mathrm{FeO}^{\mathrm{melt}}$. R is the gas constant, P in GPa, T in Kelvin. Value calculated for r_0 in first expression is used in that for E. $\gamma^{\mathrm{garnet}}_{\mathrm{Fe}}$ from Eq. 14 of van Westrenen et al. (this issue)

tical D_0 expression may be preferable to some users. One major advantage of the thermodynamic expression is that P and T are explicitly incorporated. This allows direct application to polythermal, polybaric partial melting processes involving garnet or majorite, whereas an additional model for the Fe–Mg K_D dependence on P and T is required to use the statistical D_0 expression in these cases.

At the completion of our statistical evaluations, we were unable to isolate a variable that can tie D_0 explicitly to majorite content in garnet. The variables we chose that might have yielded such a link were Si and Al per formula unit, Al–Si K_D, and perhaps pressure. None of these survived our criteria for successful regression analysis. This is fully consistent with the thermodynamic analysis in our companion paper (van Westrenen and Draper, this issue).

Comparison between model and measurements

In Table 8 and Fig. 3 we present comparisons between measured D values and those predicted from the updated model. Table 8 lists percent relative mismatches between model predictions and measurements for trivalent cation partitioning, defined as

$$\frac{|D_{\text{predicted}} - D_{\text{measured}}|}{D_{\text{measured}}} \times 100,$$

where $D_{\text{predicted}}$ is the D value for a given cation predicted from the model equations, D_{measured} is the measured value, and the absolute value of the difference is used in the numerator. Table 8 provides the minimum, maximum, and average mismatches for each element, for both cases where the thermodynamic and the statistical expressions for D_0 are used (recall that E and r_0 are always predicted using the thermodynamic relations). For most elements, the average mismatch is on the order of a few tens of percent relative. Note that for seven elements (Ce, Nd, Sm, Gd, Dy, Er, and Lu), the use of the statistical D_0 expression yields lower or equal maximum and average mismatches, whereas for the thermodynamic D_0 case, Sc, Y, Eu, and Yb have the lowest average mismatches. Values for Gd, Dy, and Er are essentially indistinguishable between the two cases.

Partitioning data for trivalent cations from nine experimental runs selected (essentially at random) from the studies listed in Table 1 are plotted against ionic radius in Fig. 3 and compared with model curves derived both from the original WvW01 formulation and from the current work. In Fig. 3a, data from two experiments performed under nominally anhydrous conditions at ~3 GPa on basaltic (Salters and Longhi 1999) and eclogitic (Pertermann et al. 2004) starting materials are well matched by the new model curves, with significant improvement over the WvW01 model. Note that both of these experiments lack data for Sc, and hence were not included in the statistical database. A slight mismatch persists between the model predictions and the data from the Salters et al. (2002) experiment, although we note that the mismatch is less than it was for the WvW01 model. This panel illustrates that the new model performs as well or better than did the original WvW01 formulations for generally basaltic systems typical of melting in Earth's mantle.

In Fig. 3b, we plot data from two nominally anhydrous experiments on Fe-rich bulk compositions relevant to extraterrestrial petrogenesis, performed at 3–5 GPa. Both data sets were included in the statistical database, because the number of garnet partitioning data from such systems is extremely limited (Draper et al. 2003, 2006). Unsurprisingly, the new model does an excellent job of accounting for these measurements, and again constitutes a substantial improvement over the mismatches with the WvW01 formulations (see also Fig. 1). Thus it would appear that garnet partitioning in anhydrous, Fe-rich systems appropriate for lunar or martian petrogenesis can be accounted for by the new formulation, although full confirmation awaits the appearance of new data in Fe-rich systems not included in the present database.

Figure 3c, d illustrate where the new model succeeds less well than in the above cases. In Fig. 3c, we plot data from two hydrous experiments on basaltic (Barth et al. 2002) to intermediate (Nicholls and Harris 1980) compo-

Table 8 Percent relative mismatches between measured partitioning values and model predictions

	Sc	Y	Ce	Nd	Sm	Eu	Gd	Dy	Er	Yb	Lu
Thermodynamic E, D_0											
Minimum mismatch	1.2	2.8	39.0	3.9	5.9	0.3	1.7	0.1	0.5	0.6	6.6
Maximum mismatch	121.1	115.2	94.2	176.1	129.4	120.7	43.7	176.6	57.6	128.7	74.4
Average mismatch	35.8	42.5	75.0	59.8	45.9	37.3	22.2	43.6	30.3	40.3	42.8
Thermodynamic E, statistical D_0											
Minimum mismatch	0.3	0.6	17.0	0.1	1.2	3.0	5.5	0.4	1.3	0.0	4.6
Maximum mismatch	168.8	284.3	94.2	92.6	98.6	103.5	46.7	272.1	74.5	220.9	69.5
Average mismatch	54.8	45.0	58.8	40.8	41.1	41.3	21.1	42.3	28.3	46.9	26.7

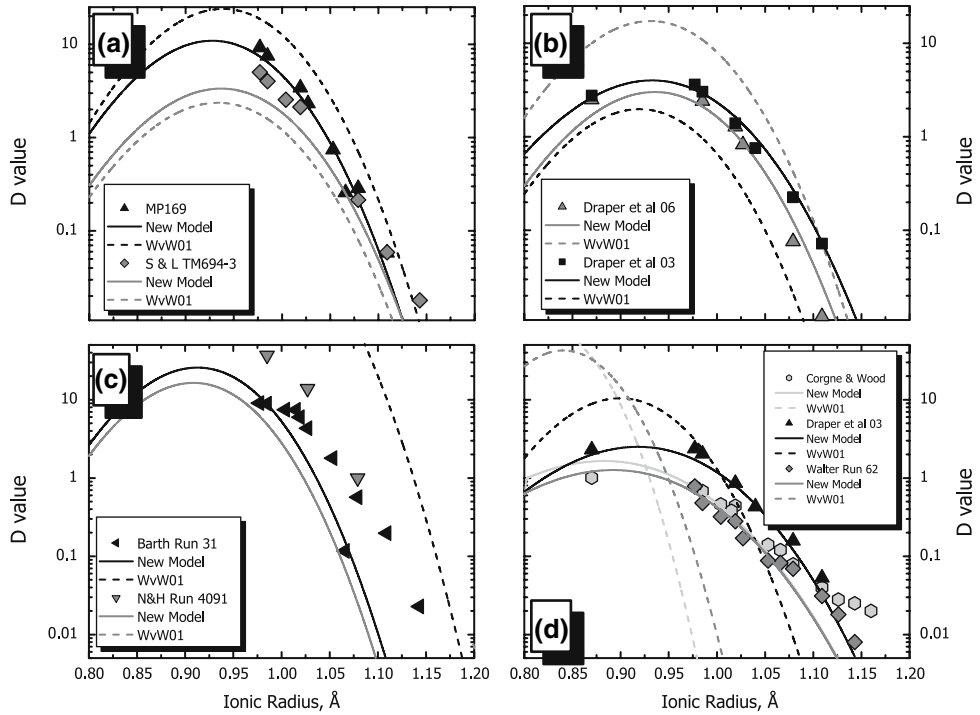

Fig. 3 Plots comparing experimental data with original WvW01 model (*dashed curves*; *WvW*01 in legends) and with updated version presented here (*solid curves*; *New Model* in legends). **a** Nominally anhydrous experiments in basaltic systems. Data from run MP169 of Pertermann et al. (2004) and run TM694-3 of Salters and Longhi (1999). Neither run included Sc data, so both were excluded from statistical database. Updated model improves upon WvW01 version for both basaltic (Salters) and eclogitic (Pertermann) compositional systems. **b** Nominally anhydrous experiments in Fe-rich systems. Data from run A140 on low-Ti lunar picrite from Draper et al. (2006) and runs 223 + 243 on Homestead L5 chondrite (5 GPa, small majorite content) from Draper et al. (2003). Both were included in statistical database. Updated model significantly improves upon WvW01 model. **c** Hydrous experiments in basaltic to intermediate systems. Data from run 31 of Barth et al. (2002) and run 4091 of Nicholls and Harris (1980). Although updated model is major improvement over WvW01, mismatch is still unacceptably large. Similar relations hold for hydrous experiments producing majoritic garnet at high pressure (Inoue et al. 2000) (not shown). **d** Nominally anhydrous experiments in ultramafic systems at high pressure, with substantial majorite content in garnet. Data from Corgne and Wood (2004), runs 233 + 244 (9 GPa, larger majorite content) of Draper et al. (2003), run 62 of Walter et al. (2004). Former two included in statistical database, latter one, lacking Sc data, was not. Model update is significant improvement over WvW01. Mismatch with largest ionic radius cations (lightest REE) in Corgne and Wood (2004) and Walter et al. (2004) experiments is attributed to minor incorporation of melt in garnet trace element analyses

sitions at 2–3 GPa. As before, we see a very significant improvement over the WvW01 model. That model drastically overestimated D_0 (4,000 to 24,000 instead of a more realistic 10–20), causing the dashed curves on this figure representing the original model to exit from the depicted D versus ionic radius space. Still, the new model yields unacceptable mismatches with the measured D values. As mentioned above, Wood and Blundy (2002) attempted to model the effect of H_2O on garnet-melt partitioning using a thermodynamic approach. The D_0 values used in their calibration were largely based on constrained fits to Sc-free experiments, using WvW01 model values for r_0 and E as boundary conditions. Owing to the relatively low temperatures involved, our new crystal-chemical formulations predict significantly lower r_0 and E values than did WvW01 for experiments containing hydrous melts. This difference is illustrated in Fig. 3c by the offset of model curves to lower ionic radius values compared to the experimental measurements, and implies that the model of Wood and Blundy (2002) may need to be re-evaluated using values of D_0 that are constrained by the new rather than old models for r_0 and E.

In Fig. 3d, we plot data from studies that produced garnets having a significant majorite content in nominally anhydrous experiments performed at 9–25 GPa. These include one experiment on Homestead L5 ordinary chondrite at 9 GPa (Draper et al. 2003); the experiment reported by Corgne and Wood (2004); and an experiment performed by Walter et al. (2004). The latter study lacked Sc data and so was not included in the statistical database, but the former two runs were included. Once again, the new model does a much better job accounting for the measured data than did the WvW01 formulation. Significant mismatches remain, particularly for high-ionic radius elements like the light rare earths, which are expected to have the smallest D values. Such elements are notoriously difficult to work with

in partitioning studies, owing to the effect of incorporation of even the smallest amounts of melt in the garnet trace element analyses. Such incorporation of melt, much richer in low-*D* elements than is coexisting garnet, can artificially raise the apparent D values for those elements (Draper et al. 2006). We attribute the departure of the LREE partitioning data of Walter et al. (2004) and Corgne and Wood (2004) from the parabolic curve to that very phenomenon. Finally, applying the new model to the single study in which majoritic garnets were produced in hydrous experiments (Inoue et al. 2000) (not shown) yields even worse mismatches than for the lower pressure hydrous data shown in Fig. 3c. The mismatches with hydrous partitioning data constitute our updated model's largest shortcoming.

Tetravalent cation partitioning

Finally, it would be highly desirable to be able to predict garnet-melt partitioning of 4+ cations to a similar level of success as we have now demonstrated for trivalent cations. Ratios of trivalent cations like the heavy rare earths to high field strength 4+ cations (e.g. Lu/Hf), as well as their isotopic systematics, are widely used geochemical fingerprints for a variety of petrologic processes in terrestrial-planet basaltic magmatism (Salters and Hart 1989; Hirschmann and Stolper 1996; Salters 1996; Beard et al. 1998; Blichert-Toft et al. 1999; Green et al. 2000; Chauvel and Blichert-Toft 2001; Klemme et al. 2002). It is much more difficult, if not impossible, to apply the lattice-strain methodology for predicting 4+ partitioning for a variety of reasons. First, there are fewer elements that meet the requirement to apply the lattice-strain model, namely having the same charge and entering the same crystallographic site, in this case likely the garnet Y-site. Hf, Ti, and Zr meet this requirement, but the ionic radii of Hf and Zr are extremely similar and are close to the expected r_0 value for 4+ partitioning into garnet's Y-site (van Westrenen et al. 2001a). Thus, data for additional elements with radii significantly lower and higher than these are needed. Elements with larger ionic radii include Th and U, but these are too large to fit into the Y-site, and U in addition can exist in several valence states over the range of oxygen fugacities common to most magmas. On the smaller side of the lattice-strain parabola, there are virtually no 4+ elements to work with; one possibility would be to estimate the *D* value for octahedral Si entering into the Y-site for majoritic garnets, but doing so is complicated by our lack of knowledge of how much of the Si in the liquid phase is also octahedrally coordinated. In addition, there is some evidence that some 4+ cations, such as Zr and Hf, may enter into both X- and Y-sites in the garnet structure (van Westrenen et al. 2001a). It is therefore not feasible to evaluate lattice-strain fit parameters for 4+ cations in the same manner as we outlined above for 3+ cations.

In the absence of lattice-strain fit parameters, we used the same variable subsets identified as being linearly independent by our bivariate correlation analysis (Tables 3, 4, 5) in multiple linear regressions with the literature Ti, Hf and Zr *D* values themselves. These regressions sought to determine whether those subsets could be used to predict directly these partition coefficients. Unfortunately, none of these attempts was successful. In all cases, multiple correlation coefficients and their associated coefficients of determination were very low, ranging from approximately 0.1 to 0.2. It is therefore clear that more detailed work will be required if a predictive model for garnet-melt partitioning of 4+ cations is to be achieved.

Conclusions and future directions

We have developed a new predictive model for garnet-melt partitioning of trivalent cations to be used to model anhydrous partial melting processes under a variety of conditions and bulk compositions relevant to Earth, Moon, and Mars. Data from water-bearing experiments are only poorly reproduced, both for lower pressure systems where garnet is largely pyropic, and for higher pressure conditions where garnet incorporates a significant majorite component.

The model has been successfully applied to anhydrous data from experiments up to 9 GPa. There is a lack of accurate partitioning data between this pressure and the majoritic garnet stability limit of ~25 GPa that remains to be filled by subsequent experimentation. No parameter explicitly connected to the increasing majorite content in garnet with increasing pressure was found to be statistically significant, although our crystal-chemical model for *E* (van Westrenen and Draper this issue) does incorporate such a term. Nevertheless, mismatches between measurements in majoritic garnet and our updated model are much smaller than the mismatches between measurements and the WvW01 version. We suggest that when the pressure gap is filled, we will have data reflecting the gradual transition to majorite from lower pressure pyropic garnets, and this enhanced coverage may allow us to account better for the onset of the majorite transition.

Accordingly, the next steps in achieving a predictive model that can handle virtually all compositional factors and apply to petrogenesis anywhere on the terrestrial planets should include (1) greater coverage of the pyrope-to-majorite transition; (2) more complete coverage of pressures between ~9 and 25 GPa; and (3) a systematic effort to understand the effect of water of a scale similar to the one mounted thus far in anhydrous systems, aimed at

improving upon the initial garnet-hydrous melt calibration of Wood and Blundy (2002) as described earlier. We speculate that the role of water will also help elucidate the effects of melt composition and structure, given the profound effects the presence of water has on melting and crystallization reactions in magmatic systems.

Acknowledgments We are grateful to Dr. Charles K. Shearer and Mr. Paul V. Burger for invaluable assistance in performing trace element analyses using the University of New Mexico SIMS facility, and to Mr. Michael Spilde for his help with electron microprobe analyses in UNM's electron beam laboratory. Journal reviews by an anonymous reviewer and, especially, by Dr. Marc Hirschmann greatly improved this paper. This research was supported by National Science Foundation grant EAR-0337237 to DSD and a European Young Investigator (EURYI) award to WvW.

References

Barth MG, Foley SF, Horn I (2002) Partial melting in Archean subduction zones; constraints from experimentally determined trace element partition coefficients between eclogitic minerals and tonalite melts under upper mantle conditions. Precambrian Res 113:323–340

Beard BL, Taylor LA, Scherer EE, Johnson CM, Snyder GA (1998) The source region and melting mineralogy of high-titanium and low-titanium lunar basalts deduced from Lu-Hf isotope data. Geochim Cosmochim Acta 62:525–544

Beattie P, Drake M, Jones J, Leeman W, Longhi J, McKay G, Nielsen R, Palme H, Shaw D, Takahashi E, Watson B (1993) Terminology for trace-element partitioning. Geochim Cosmochim Acta 57:1605–1606

Bennett SL, Blundy J, Elliott T (2004) The effect of sodium and titanium on crystal-melt partitioning of trace elements. Geochim Cosmochim Acta 68:2335–2347

Blichert-Toft J, Gleason JD, Telouk P, Albarede F (1999) The Lu-Hf isotope geochemistry of shergottites and the evolution of the Martian mantle-crust system. Earth Planet Sci Lett 173:25–39

Blundy J, Wood B (1994) Prediction of crystal-melt partition coefficients from elastic moduli. Nature 372:452–454

Carroll MR, Draper DS (1994) Noble gases as trace elements in magmatic processes. Chem Geol 117:37–56

Chauvel C, Blichert-Toft J (2001) A hafnium isotope and trace element perspective on melting of the depleted mantle. Earth Planet Sci Lett 190:137–151

Corgne A, Wood BJ (2004) Trace element partitioning between majoritic garnet and silicate melt at 25 GPa. Phys Earth Planet Inter 143–144:407–419

Dowty E (1980) Crystal-chemical factors affecting the mobility of ions in minerals. Am Mineral 65:174–182

Draper DS, Xirouchakis D, Agee CB (2003) Trace element partitioning between garnet and chondritic melt from 5 to 9 GPa: Implications for the onset of the majorite transition in the Martian mantle. Phys Earth Planet Inter 139:149–169

Draper DS, du Frane SA, Dwarzski RE, Shearer CKJ, Agee CB (2006) High-pressure phase equilibria and element partitioning experiments on Apollo 15 green C picritic glass: Implications for the role of garnet in the deep lunar interior. Geochim Cosmochim Acta 70:2400–2416

Dwarzski RE, Draper DS, Shearer CKJ, Agee CB (2006) Preliminary insights on crystal chemistry of high titanium garnets from partitioning of rare earth and high field strength elements. Am Mineral 91:1536–1546

Fortier SM, Giletti BJ (1989) An empirical model for predicting diffusion coefficients in silicate minerals. Science 245:1481–1484

Gaetani GA (2004) The influence of melt structure on trace element partitioning near the peridotite solidus. Contrib Mineral Petrol 147:511–527

Green TH, Blundy JD, Adam J, Yaxley GM (2000) SIMS determination of trace element partition coefficients between garnet, clinopyroxene and hydrous basaltic liquids at 2–7.5 GPa and 1080–1200 degrees C. Lithos 53:165–187

Hauri EH, Wagner TP, Grove TL (1994) Experimental and natural partitioning of Th, U, Pb and other trace elements between garnet, clinopyroxene and basaltic melts. Chem Geol 117:149–166

Hirschmann MM, Stolper EM (1996) A possible role for garnet pyroxenite in the origin of the "garnet signature" in MORB. Contrib Mineral Petrol 124:185–208

Inoue T, Rapp RP, Zhang J, Gasparik T, Weidner DJ, Irifune T (2000) Garnet fractionation in a hydrous magma ocean and the origin of Al-depleted komatiites; melting experiments of hydrous pyrolite with REEs at high pressure. Earth Planet Sci Lett 177:81–87

Jenner GA, Foley SF, Jackson SE, Green TH, Fryer BJ, Longerich HP (1993) Determination of partition coefficients for trace elements in high pressure-temperature experimental run products by laser ablation microprobe-inductively coupled plasma-mass spectrometry (LAM-ICP-MS). Geochim Cosmochim Acta 57:5099–5103

Johnson KTM (1994) Experimental cpx/ and garnet/melt partitioning of REE and other trace elements at high pressures; petrogenetic implications. Mineral Mag 58A:454–455

Kato T, Ringwood AE, Irifune T (1988) Experimental determination of element partitioning between silicate perovskites, garnets and liquids; constraints on early differentiation of the mantle. Earth Planet Sci Lett 89:123–145

Klein M, Stosch HG, Seck HA, Shimizu N (2000) Experimental partitioning of high field strength and rare earth elements between clinopyroxene and garnet in andesitic to tonalitic systems. Geochim Cosmochim Acta 64:99–115

Klemme S, Blundy JD, Wood BJ (2002) Experimental constraints on major and trace element partitioning during partial melting of eclogite. Geochim Cosmochim Acta 66:3109–3123

Mysen BO (1983) The structure of silicate melts. Ann Rev Earth Planet Sci 11:75–97

Mysen BO, Dubinsky EV (2004) Melt structural control on olivine/melt element partitioning of Ca and Mn. Geochim Cosmochim Acta 68:1617–1633

Nicholls IA, Harris KL (1980) Experimental rare earth element partition coefficients for garnet, clinopyroxene and amphibole coexisting with andesitic and basaltic liquids. Geochim Cosmochim Acta 44:287–308

Onuma N, Higuchi H, Wakita H, Nagasawa H (1968) Trace element partition between two pyroxenes and the host lava. Earth Planet Sci Lett 5:47–51

Pertermann M, Hirschmann MM, Hametner K, Gunther D, Schmidt MW (2004) Experimental determination of trace element partitioning between garnet and silica-rich liquid during anhydrous partial melting of MORB-like eclogite. Geochem Geophys Geosyst 5. doi:10.1029/2003GC000638

Quartieri S, Antonioli G, Geiger CA, Artioli G, Lottici PP (1999a) XAFS characterization of the structural site of Yb in synthetic pyrope and grossular garnets. Phys Chem Minerals 26:251–256

Quartieri S, Chaboy J, Antonioli G, Geiger CA (1999b) XAFS characterization of the structural site of Yb in synthetic pyrope and grossular garnets; 2, XANES full multiple scattering calculations at the Yb, LI- and LIII-edges. Phys Chem Minerals 27:88–94

Quartieri S, Boscherini F, Chaboy J, Dalconi MC, Oberti R, Zanetti A (2002) Characterization of trace Nd and Ce site preference and coordination in natural melanites; a combined X-ray diffraction and high-energy XAFS study. Phys Chem Minerals 29:495–502

Salters VJM (1996) The generation of mid-ocean ridge basalts from the Hf and Nd isotope perspective. Earth Planet Sci Lett 141:109–123

Salters VJM, Hart SR (1989) The hafnium paradox and the role of garnet in the source of mid-ocean-ridge basalts. Nature 342:420–422

Salters VJM, Longhi J (1999) Trace element partitioning during the initial stages of melting beneath mid-ocean ridges. Earth Planet Sci Lett 166:15–30

Salters VJM, Longhi JE, Bizimis M (2002) Near mantle solidus trace element partitioning at pressures up to 3.4 GPa. Geochem Geophys Geosyst 3. 2001GC000148

Shannon RD (1976) Revised effective ionic radii and systematic studies of interatomic distances in halides and chalcogenides. Acta Crystallogr A32:751–767

Shimizu N, Kushiro I (1975) The partitioning of rare earth elements between garnet and liquid at high pressures; preliminary experiments. Geophys Res Lett 2:413–416

Sisson TW, Bacon CR (1992) Garnet/high-silica rhyolite trace element partition coefficients measured by ion microprobe. Geochim Cosmochim Acta 56:2133–2136

Walter MJ, Nakamura E, Tronnes RG, Frost DJ (2004) Experimental constraints on crystallization differentiation in a deep magma ocean. Geochim Cosmochim Acta 68:4267–4284

van Westrenen W, Blundy J, Wood B (1999) Crystal-chemical controls on trace element partitioning between garnet and anhydrous silicate melt. Am Mineral 84:838–847

van Westrenen W, Allan NL, Blundy JD, Purton JA, Wood BJ (2000a) Atomistic simulation of trace element incorporation into garnets; comparison with experimental garnet-melt partitioning data. Geochim Cosmochim Acta 64:1629–1639

van Westrenen W, Blundy JD, Wood BJ (2000b) Effect of Fe2+ on garnet-melt trace element partitioning: experiments in FCMAS and quantification of crystal-chemical controls in natural systems. Lithos 53:189–201

van Westrenen W, Blundy JD, Wood BJ (2001a) High field strength element/rare earth element fractionation during partial melting in the presence of garnet: Implications for identification of mantle heterogeneities. Geochem Geophys Geosys 2. 2000GC000133

van Westrenen W, Wood B, Blundy J (2001b) A predictive thermodynamic model of garnet-melt trace element partitioning. Contrib Mineral Petrol 142:219–234

Wood BJ, Blundy JD (1997) A predictive model for rare earth element partitioning between clinopyroxene and anhydrous silicate melt. Contrib Mineral Petrol 129:166–181

Wood BJ, Blundy JD (2002) The effect of H_2O on crystal-melt partitioning of trace elements. Geochim Cosmochim Acta 66:3647–3656

Xirouchakis D, Draper DS, Agee CB (2002) The garnet to majorite transformation in mafic compositions. Lunar Plan Sci XXXIII:abstract#1316

Yurimoto H, Ohtani E (1992) Element partitioning between majorite and liquid; a secondary ion mass spectrometric study. Geophys Res Lett 19:17–20